Design strategies for the self-assembly of polyhedral shells

Diogo E. P. Pinto[a], Petr Šulc[b,c] [iD], Francesco Sciortino[a] [iD], and John Russo[a,1] [iD]

The control over the self-assembly of complex structures is a long-standing challenge of material science, especially at the colloidal scale, as the desired assembly pathway is often kinetically derailed by the formation of amorphous aggregates. Here, we investigate in detail the problem of the self-assembly of the three Archimedean shells with five contact points per vertex, i.e., the icosahedron, the snub cube, and the snub dodecahedron. We use patchy particles with five interaction sites (or patches) as model for the building blocks and recast the assembly problem as a Boolean satisfiability problem (SAT) for the patch–patch interactions. This allows us to find effective designs for all targets and to selectively suppress unwanted structures. By tuning the geometrical arrangement and the specific interactions of the patches, we demonstrate that lowering the symmetry of the building blocks reduces the number of competing structures, which in turn can considerably increase the yield of the target structure. These results cement SAT-assembly as an invaluable tool to solve inverse design problems.

nanotechnology | capsids | self-assembly | SAT

Self-assembly encompasses a large array of phenomena through which materials are formed using simple microscopic building blocks (1). In nature, many striking examples of self-assembly are found, from virus capsids to lipid bilayers (2–6), but assembling new synthetic materials has proved to be very challenging. Successful examples of artificial self-assembly have required a large dose of educated guesses (7–24). One of the main difficulties resides in how to optimize the geometrical properties or the interactions between the building blocks without leading to competing or kinetically arrested configurations (25–28).

Here, we focus on the self-assembly of finite-size structures and in particular on specific polyhedral shells. From an application standpoint, the potential of closed shells to act as a drug delivery system has been a widely researched topic, where a given drug is encapsulated within a closed shell and then driven to a specific diseased area where the drug is locally released such that the least amount of nondiseased tissue is affected (29, 30). For this, the shell needs to close around a specific reagent and then open when external conditions are met. Recently, there have been suitable experimental realizations, for example, using DNA-origami, where selective interactions can be introduced to mimic patchy particles (31–35).

When focusing on finite-size shells, additional challenges arise compared to the ones encountered in the self-assembly of crystal structures. First, the self-assembly occurs exclusively from the gas phase, which rules out the possibility to use (critical point induced) density fluctuations to accelerate the rate of aggregation (36), as frequently done in the case of crystals. On the contrary, the formation of finite-size aggregates stabilizes the gas phase to high densities with respect to the liquid phase, possibly introducing a density dependence of the aggregation pathway. Second, the small size of the aggregates, compared to the infinitely repeating units of a crystal, can stabilize kinetic traps, i.e., structures whose free energy is not as low as the one of the target structure but that require an exceedingly long waiting time to break. Lastly, the formation of finite-size aggregates is a continuous process and is not accompanied by a phase transition as in crystals. The absence of a critical size of formation (i.e., the critical nucleus) means that it is not sufficient to suppress a handful of competing structures at one length scale but that the assembly process has to proceed without defects at every stage. This problem is reflected in the difficulty of perfectly closing large-size aggregates, such as capsids (31).

Here, we show how to successfully tackle these challenges by transforming the self-assembly problem into a Boolean satisfiability problem. This technique, named SAT-assembly, was recently introduced by some of us to successfully assemble challenging crystalline structures, with an emphasis on structures that have photonic applications, such as the tetrastack (37) and diamond cubic crystal (37–39), and structures with a high number of atoms in the unit cells, such as clathrate crystals (37). The SAT-assembly

Significance

Nature is able to self-assemble complex supramolecular structures from elementary building blocks rarely making mistakes. For example, adenovirus nucleocapsids are formed from different proteins that assemble and fold into a regular icosahedral shell. One of the goals of nanotechnology is to emulate these strategies to produce new synthetic materials. Unfortunately, most artificial designs fail because the units misassemble into incorrect, and often irregular, structures. We here propose a design strategy for self-assembling finite-size shells where the interaction between the units is obtained from the solution to a Boolean satisfiability problem (SAT). We demonstrate that this quite general approach excels in self-assembling different Archimedean polyhedral shells with high yield, revealing some general rules guiding the design of successful assembles.

design pipeline allows for a fast search of design space for solutions that can form desired target structures and—equally important—avoid undesired alternative assemblies or kinetic traps. In this article, we will demonstrate a successful application of the SAT-assembly framework to the assembly of complex polyhedral shells. We focus on the three polyhedra that can assemble from building blocks with a coordination number of five, i.e., the icosahedron, the snub cube, and the snub dodecahedron. As building blocks we use patchy particles, which are a model of hard spheres with attractive patches on their surface (22, 40–45). These represent a coarse-grained approach to describe multiple systems, e.g., colloids, proteins, polymers, DNA origami (14, 15, 39, 46, 47). By associating to each patch a color, we can translate the self-assembly problem into the problem of finding how patch colors should interact to form the target structure, while at the same time avoiding competing structures. It is possible that different natural structures follow similar strategies to the examples explored here, with focus on selectivity. For example, adenoviruses are known for their icosahedral nucleocapsid which is assembled by two main proteins and three minor ones that mostly influence the interactions (48). As such, these processes evolved to require a minimum level of specificity in the building blocks and interactions in order to form regular shells.

In the manuscript, we will first show that, except for the smallest structure (the icosahedron), these shells do not assemble correctly if only the geometrical information about the target structure (the "educated guess") is used. Instead, we will introduce multicolored designs, i.e., designs where more than one patch type is present. As the number of patch types increases, so does the complexity of the design, making SAT a necessary tool to be able to find the desired interactions between patch colors that can form the target shell and avoid alternative assemblies. We will show that the yield of the different structures depends sensitively, in addition to the particular geometrical patch arrangement, on the number of colors used but that the different results can be rationalized by looking at the symmetry of the designs: Less symmetrical building blocks self-assemble with the highest yield in the target structures. In particular, *chiral* designs, i.e., not having a mirror-plane symmetry, are found to be very effective building blocks regardless of the chirality of the target structure. We also explore the role of geometrical frustration, where the angle between the patches does not match the angle between the particles in the target structure, to create designs where the target structure depends on external conditions (in our case the concentration of building blocks). We also emphasize how SAT is crucial to assemble a given structure while excluding competing ones. We find that mutual exclusion requires complex designs, with multiple patch colors and particle species (different patch color arrangement in different particles), which lead to higher yields and assemblies that are more robust to geometrical frustrations. Lastly, we discuss how increasing the number of colors and species can slow down the short-time kinetics of the assembly process, which emphasizes the design principles discussed here to reach optimal results.

1. Models

We consider a system composed of N patchy particles in a cubic box of length L. The particles are characterized by a hard core of diameter σ with five patches on its surface located on one side of the particle forming a star-like shape with mirror symmetry along one of the patches (as seen in the center of Fig. 1). We follow the same SAT formulation as the one in ref. 38. We consider that each patch can have a given color x_c between $1 \leq x_c \leq N_c$,
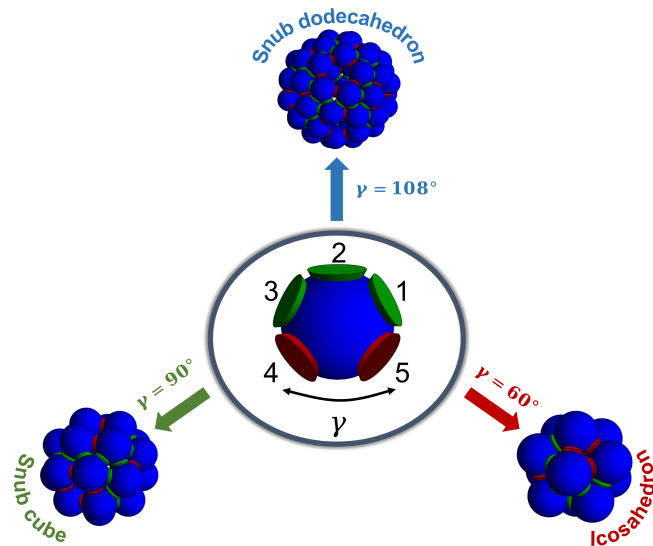

Fig. 1. Schematic representation of the three Archimedean structures with five contact points per vertex and of a valence-five particle with two types of patches (green and red) which according to the SAT algorithm can assemble into the three different polyhedron shells. Note that, in this specific design, the green patches only interact with green while the red patches only interact with red. γ indicates the in-plane angle between the two red patches.

where N_c is the total number of distinct colors. These colors can be distributed onto the patches in specific arrangements, each unique sequence can be considered a particles species x_p, thus $1 \leq x_p \leq N_p$, where N_p is the total number of distinct species. SAT is then used to find if a given combination of N_p and N_c can satisfy a given polyhedral shell, e.g., if it satisfies the topological constraints of the target structure, and to find how the colors are arranged on the different species. In *SI Appendix*, we go into more detail on the different constraints (clauses) used in SAT.

We study the self-assembly outcome of our designs focusing on the static yield, defined as the ratio of the number of fully formed target structures over the total number of aggregates. This quantity is measured once the bond probability has reached a (metastable) equilibrium state, that in our case is obtained via Monte Carlo simulations using aggregation-biased moves and using the Kern–Frenkel potential (49, 50) to describe the interaction between patches (*Methods*). In Section 3D, we also consider the short-time aggregation kinetics of our designs, i.e., the rate at which particles form aggregates from the solution. To study this we use Molecular Dynamics simulations using a continuous version of the Kern–Frenkel potential (*Methods*).

Our self-assembly problem is represented schematically in Fig. 1. Starting with patchy particles of valence five, we wish to selectively assemble three Archimedean polyhedral shells: the 12-particle *icosahedron*, the 24-particle *snub cube*, and the 60-particle *snub dodecahedron*. In the ideal structure, three contact points (patches 1, 2, and 3) are in the same location in all three polyhedral shells, making an in-plane angle with the center of the particle of 60°, while the other two contact points differ for the in-plane angle that patches 4 and 5 make with the center of the particle, which we call γ. Note that in the ideal structure, $\gamma = 60°$ for the icosahedron, $\gamma = 90°$ for the snub cube, and $\gamma = 108°$ for the snub dodecahedron. We consider two geometrical control parameters: the angular width of the patch interaction, $\cos\theta_{\max}$, and the in-plane angle γ. In addition to the geometrical parameters, we investigate different SAT solutions, i.e., different number of particle types and different colors among the five patches. As alluded before, the SAT-assembly algorithm

provides an interaction table among the colors such that all bonds in the target structure(s) are satisfied. Finally, we also vary the temperature and density conditions of the assembly to study the phase behavior of the different designs.

Unless stated otherwise, the temperature used is $T = 0.097$. This value is high enough to guarantee that we are above the critical micelle concentration for the densities explored (*SI Appendix*). It also guarantees that bonds are able to break at a reasonable pace during the simulations but still persist long enough for structures to form especially in more dilute systems. For the densities explored, this value also guarantees that we are always close to the ideal gas phase of fully formed aggregates (*SI Appendix*). Temperature (T) is expressed in units of ε, the patches binding energy, and $k_B = 1$, while all lengths are in units of σ.

2. The "Educated Guess": Geometrical Designs

To consider geometric effects only, we fix one patch color (i.e., each patch can interact with all others) and explore different values of the patch width, $\cos\theta_{max}$ as well as different geometries of the patches by changing the in-plane angle γ.

The former parameter allows for more flexibility of the bonds due to larger patch widths. The latter improves our ability to target the different structures proposed in Fig. 1 by more easily satisfying their geometry.

Fig. 2 summarizes the results, showing the most probable closed structure assembled for each value of $\cos\theta_{max}$ and γ considered. As represented by the triangle symbols (and the shaded area), we find that only the icosahedron is able to form for the range of parameters explored, while the snub cube and snub dodecahedron fail to assemble even when the geometry of the particles is the ideal one ($\gamma = 90°$ for the snub cube, and $\gamma = 108°$ for the snub dodecahedron).

We classify the state points where no target structure is formed into two groups. The gray stars correspond to irregular aggregates, thus clusters more akin to micelles, that close without defects but
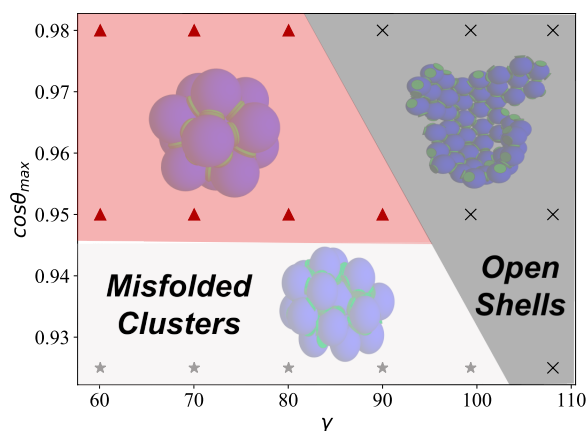
do not have a regular shape. If no closed structure is formed, we use black crosses to classify the state point, the ones where particles form bonds but they do not close, thus forming an open shell.

These results confirm the well-known fact that self-assembly designs cannot generally rely only on the geometrical properties of the building units alone. In our case, only the smallest target structure, the icosahedron, is successfully self-assembled. The assembly is limited up to $\gamma \sim 90°$, above which the geometry of the building unit is not compatible with bond formation in the target structure and only incomplete structures are formed. As expected, the γ range increases for increasing patch width (lowering $\cos\theta_{max}$). But crucially, the assembly is also limited at large patch widths, $\cos\theta_{max} > 0.95$, below which mostly irregular structures are observed. With large patch widths, there are multiple ways for a shell to close onto itself, and this degeneracy entropically stabilizes irregular structures over the more ordered polyhedral shells. We note that although icosahedron structures are still observed for large patch widths, $\cos\theta_{max} < 0.95$, a lot fewer are completely assembled (less than 5%).

3. SAT Designs

A. Patch Coloring. In contrast to the previous section, we now break the interaction symmetry and introduce patch colors. We start by considering a solution that satisfies all three polyhedral structures with only one particle species ($N_p = 1$) and two patch colors ($N_c = 2$). We employ SAT to satisfy such constraints and extract the proper patch ordering and interactions. The SAT solution, represented schematically in Fig. 1, allows only interactions among patches of the same color (green with green, red with red): 1, 2, and 3 (green) on one side and 4 and 5 (red) on the other.

In Fig. 3, we display the results for this design, showing which structures are formed depending on the geometrical parameters $\cos\theta_{max}$ and γ. Comparing these results with Fig. 2, we observe that all three polyhedral shells can be assembled within the parameters explored. Differently from before, the structures form at all values of $\cos\theta_{max}$ considered, and the dominant structure is controlled primarily by the angle γ, with the stability of each structure approximately centered around its optimal angle. As observed before, structures with fewer particles are favored when the patch width increases: This is an entropic effect, as fully formed shells behave as an ideal gas of clusters, whose entropy increases with number density of clusters. Snapshots of the gas of icosahedral, snub cube, and snub dodecahedron are shown in the upper panels of Fig. 3.

Already from the results of Fig. 3, we can assert that even the introduction of minimal patch coloring significantly improves the self-assembly process. In the next section, we will look in detail the effects of different coloring patterns on the yield of self-assembly.

B. Patch Patterning. The table in Fig. 4 contains seven different patch patterning designs, varying the number of colors and the interaction among them. As the number of colors increases, so does the complexity of the design. As such, SAT-assembly frameworks becomes essential to assign the color interactions such that all desired target structures are possible. The name of the design expresses the number of colors used and, in parenthesis, different patterning choices: for example, $C4(1)$ and $C4(2)$ are two different designs with four colors. Each design is compatible with all three target structures, and we test them

Fig. 2. Most probable structure formed for different in-plane angles, γ, and for different patch widths, $\cos\theta_{max}$, when all patches are identical. The triangles inside the red region represent parameters where the polyhedron forming with the highest yield is the icosahedron. Black crosses represent parameter values where open/incomplete clusters are more probable. The gray stars represent systems where closed clusters are able to form, but none of them is an Archimedean five-coordinated polyhedron. Thus, for the one-patch type "educated guess" solution, only the icosahedron is able to form. Results refer to $T = 0.097$ and $\rho = 0.01$. Temperature (T) is expressed in units of ε and $k_B = 1$, while all lengths are in units of σ.
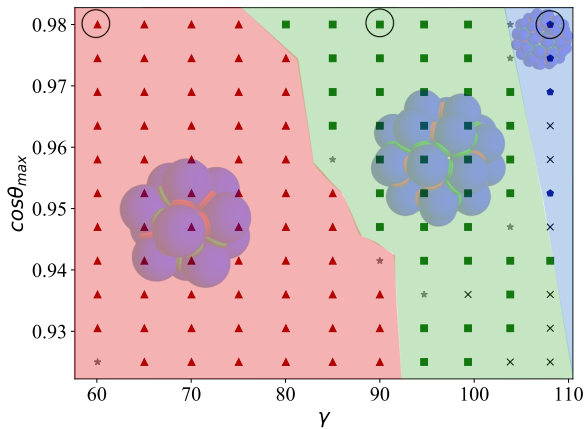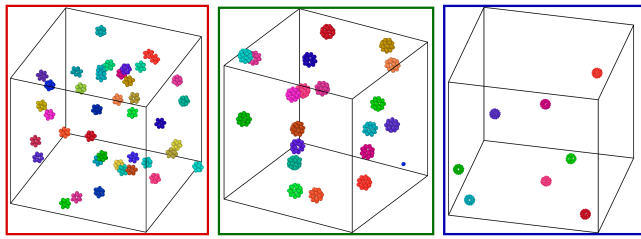
Fig. 3. *Top*: Snapshots of the final configurations obtained from simulations based on a one-component system (corresponding to the circles in the main diagram). Particles have two types of patches (red and green) and bind via self-complementary interactions (red with red and green with green). In all simulations, $\cos\theta_{max} = 0.98$ and the $\gamma = 60, 90,$ and $108°$, respectively, i.e., at the optimal value for the three selected structures. The simulations for the icosahedron and snub cube were done with $T = 0.097$ and $\rho = 0.01$, while for the snub dodecahedron, $\rho = 0.001$ was used. In all snapshots, the yield of the most probable shell is close to 100%. *Bottom*: Most probable structure formed for different in-plane angles, γ and for different patch width, $\cos\theta_{max}$. The triangles inside the red region represent parameters where the most probable structure is the icosahedron. The squares inside the green region represent parameters where the most probable structure is the snub cube. The pentagons inside the blue region represent parameters where the most probable structure is the snub dodecahedron. Black crosses represent systems where only open/incomplete clusters are formed. The gray stars represent systems where clusters are able to close but none correspond to the ones in Fig. 1. Results were calculated for $T = 0.097$ and $\rho = 0.01$. Temperature (T) is expressed in units of ϵ and $k_B = 1$, while all lengths are in units of σ.

for three geometrical arrangements of the patches, differing for their angle $\gamma \in [60°, 90°, 108°]$. It is important to note that for $\gamma = 60°$, all patches are geometrically indistinguishable, i.e., the angle between any two adjacent patches and the center of the particle is always $60°$. For the other values of γ, instead, the only geometric symmetry of the particles is a vertical mirror plane. This last symmetry can be broken by introducing patch coloring. By color symmetry, we refer to the presence of symmetry elements (in our case the vertical mirror plane) which bring a specific design into self-coincidence after (eventually) exchanging the identity of the colors. For example, let's consider the design C3(1) in Fig. 4: patches $(1, 2, 3)$ are green, patch 4 is red, and patch 5 is orange. The design has color symmetry because after reflecting all patches through the vertical mirror plane, and after the following color exchange (red $\leftrightarrow$ orange), both in the particle's design and in the interaction table, the solution is the same.

In the following, we will investigate how color symmetry and the total number of distinct colors used affect the self-assembly yield.

In Fig. 4, we plot the density dependence of the yield for all designs and for $\gamma = 60°$ (panel *A*), $\gamma = 90°$ (panel *B*), and

$\gamma = 108°$ (panel *C*). We define the yield as the probability of finding a cluster corresponding to a specific structure. We count single particles as a cluster of size one and any bonded particles as clusters of size two or above, depending on the number of particles bonded. For example, panel *A* shows the probability of finding a cluster that forms an icosahedron, thus the number of icosahedra formed over the total number of clusters. We stress the fact that we measure the equilibrium yield, i.e., the yield after long waiting times, as the implemented AVB-biased moves allow the particles to rapidly form bonds regardless of the system density.
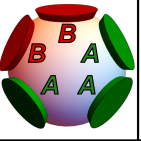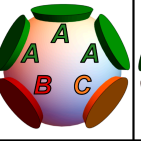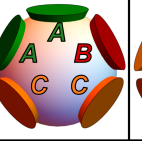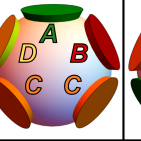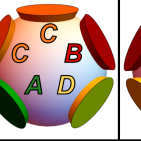
We can summarize the results of Fig. 4 with the following observations:

1. Increasing the Number of Colors Increases the Yield. Regardless of the target structure, and with few exceptions detailed below, the yield increases with the number of colors used. The increase is more significant for the first few colors added, while the yield's gain is more modest when the maximum number of colors is reached for a given number of species (in our case, the maximum number of colors is five times the number of different particle species).

This is due to the fact that the probability of creating an undesired bond, i.e., interaction between compatible patches which however creates a particle cluster whose topology (graph of all formed bonds) is not a subset of the target shape, decreases with increasing number of colors. For example, in the C2(1) design, the top patches can form three possible connections, and thus the probability that the top three green patches form a desired bond is one-third, while for the two red bottom ones is one-half. The probability of assembling the desired bonds to a central particle is then $(1/3)^3(1/2)^2 \sim 0.009$. As the number of colors increases so does the probability that a desired bond is formed. So for the C5 design, there is only one possible bonding partner for each patch, and so the only allowed bond topology is the one of the target structure.

2. Decreasing the Symmetry of the Building Block Increases the Yield. While for $\gamma = 60°$ the particles have a five-fold symmetry axis, altering the γ angle orients the particles, making all patches distinguishable. The best examples are designs C2(1) and C2(2), which are indistinguishable for $\gamma = 60°$ (panel *A*) and whose yield increases significantly going from $\gamma = 60°$ (panel *A*) to $\gamma = 90°$ (panel *B*). Notice that the design C3(1) has a similar yield for $\gamma = 60°$ (panel *A*) and $\gamma = 90°$ (panel *B*). To understand this behavior, we next introduce the concept of *color symmetry*.

3. Decreasing the Color Symmetry of the Patches Increases the Yield. As mentioned before, all designs for $\gamma \neq 60°$ have a single geometrical mirror plane, but patch coloring can maintain or break this symmetry. The designs that break the mirror-plane symmetry are *chiral* designs: C2(2), C3(2), C4(1), C4(2), and C5. The designs that preserve the mirror-plane symmetry are *achiral* designs: C2(1) and C3(1). Among the target structures, the icosahedron is an achiral assembly, while both the snub cube and the snub dodecahedron are chiral assemblies. We observe how in all cases chiral designs have higher yield compared to the achiral ones. This is true also for the icosahedron despite the lack of chirality in the target structure. For the snub cube and the snub dodecahedron, we even observe that the yield of the chiral design C2(2) is higher than the achiral design C3(1) despite using less colors. Coloring reduces the symmetry of the target structure, which in turn reduces the number of degenerate structure that can form during the assembly. Controlling the coloring of the patches is thus an effective strategy to increase the yield of the assembly.

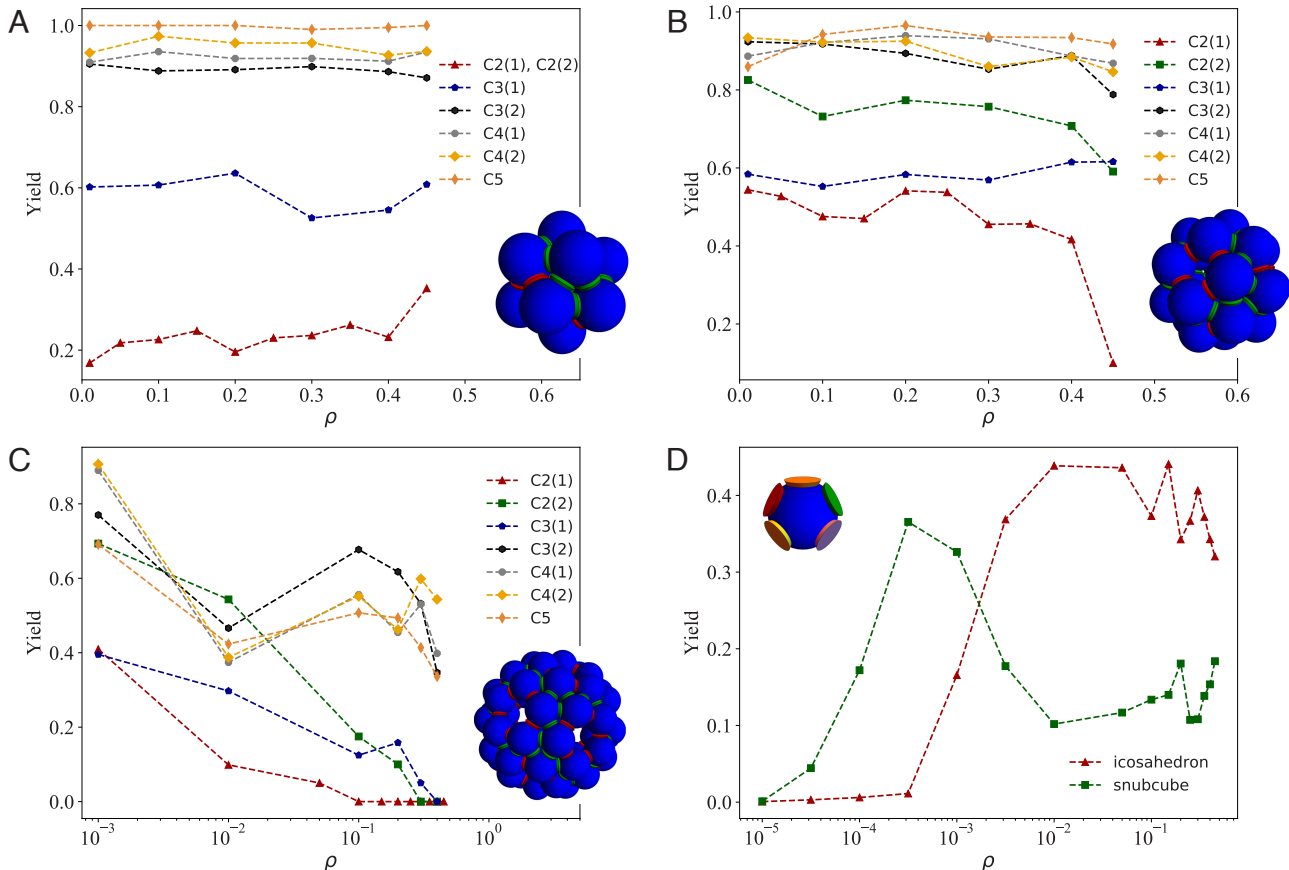| Solution	C2(1)	C2(2)	C3(1)	C3(2)	C4(1)	C4(2)	C5
Design							
Interaction	$A \leftrightarrow A$ $B \leftrightarrow B$	$A \leftrightarrow A$ $B \leftrightarrow B$	$A \leftrightarrow A$ $B \leftrightarrow C$	$A \leftrightarrow A$ $B \leftrightarrow B$ $C \leftrightarrow C$	$A \leftrightarrow D$ $B \leftrightarrow B$ $C \leftrightarrow C$	$A \leftrightarrow D$ $B \leftrightarrow B$ $C \leftrightarrow C$	$A \leftrightarrow A$ $B \leftrightarrow C$ $D \leftrightarrow E$

Fig. 4. *Top*: Graphic representation of the different one-component SAT solutions explored in this study, clarifying the respective patch coloring and interactions rules. Average yield of the icosahedron (*A*), snub cube (*B*), and snub dodecahedron (*C*) as a function of the density of patchy particles. These results were calculated with $\cos\theta_{max} = 0.98$ and the in-plane angle, γ, was chosen to be the best for each structure. Thus, the icosahedron curve was calculated with $\gamma = 60°$, the snub cube with $\gamma = 90°$, and the snub dodecahedron with $\gamma = 108°$. (*D*) shows the average yield as a function of density for the design of five colors, C5. Here, both curves were measured for the same system with $\gamma = 85.45°$ and $\cos\theta_{max} = 0.947$. All results shown in this figure were calculated at $T = 0.097$. Temperature (*T*) is expressed in units of ε and $k_B = 1$, while all lengths are in units of σ.

4. The Yield Has Only a Weak Density Dependence. We observe that the yield of the different structures is constant with density. This means that clusters are fully formed in our thermodynamic conditions and have ideal-gas behavior. Only at high densities, the yield starts decreasing, in correspondence with intercluster interactions and possibly a phase change to a liquid. Interestingly, we also observe that large structures like the snub dodecahedron, which is composed of 60 particles, are more easily assembled in very dilute systems where larger shells have more space to grow without influencing each other.

5. Frustrated Designs Allow to Target Different Structures Depending on Thermodynamic Conditions. In Fig. 4*D*, we plot the yield for the frustrated C5 design in which $\gamma = 85.26°$, thus it does not ideally satisfy any of the structures discussed previously but—given the used patch width—the icosahedron and snub cube can still be assembled. The in-plane angle, $\gamma = 85.26°$, is close to

the ideal angle for the assembly of the snub cube, which is indeed the most stable structure at low densities. However, by increasing the density, we observe a switch to the smaller icosahedral shells. While the icosahedron has a much larger free energy of formation compared to the snub cube (due to the angle being unfavorable to the icosahedron), at high density this is compensated by the translational free energy (i.e., the ideal gas free energy), which is higher for the icosahedron (having a higher number density of clusters compared to the snub cube). The possibility to switch between different target structures as a function of external control parameters is a property of experimental interest.

We note on passing that several thermodynamic properties, including the critical micelle concentration, have been evaluated for all these single-species designs. The results are discussed in detail in *SI Appendix*.

C. SAT-Assembly Selection: Eliminating Competing Structures.

In the previous examples, control over the target structure was obtained either geometrically (by changing the angles γ and θ_{max} as in Fig. 3) or thermodynamically (by changing the density as in Fig. 4D). Here, we demonstrate that SAT-assembly allows to encode structure selection directly into the patch coloring. In particular, we look for designs that satisfy only the icosahedron but not the snub cube and snub dodecahedron, and vice versa. We find that the mutual exclusion of all three target structures requires at least two particle species for the snub cube and icosahedron but four species for the snub dodecahedron. Here, we show results with two species ($N_p = 2$) and five colors ($N_c = 5$) for the icosahedron and snub cube and four species ($N_p = 4$) and twelve colors ($N_c = 12$) for the snub dodecahedron, even if other solutions with different number of colors also exist. The results with our selected designs are shown in Fig. 5. For the two-species design, we highlight that a mutually exclusive selection of the target structures can be achieved via nontrivial patch color ordering using SAT.

Comparison with the 1-species solution (Fig. 3) shows that suppression of the competing structure significantly enlarges the range of parameters where a certain shell is formed. Finally, the absence of competing structures also increases the yield to almost 100% in some regions of the parameter space for the icosahedron and to 50% for the snub cube and snub dodecahedron (*SI Appendix*).

Incidentally, we note that targeting only the snub dodecahedron is complicated by the fact that all two-species designs found by SAT are compatible with the formation of icosahedron or snub cube structures from only one of the two species, practically preempting the formation of the target structure. Using the SAT framework, we proved that no solution exists with only 2 particle species. As such, the number of species needs to be increased in order to find a suitable design that satisfies the snub dodecahedron while completely excluding the others. We found that a four-species design satisfies the constraint. Indeed, using SAT, one can calculate a solution for the snub dodecahedron and then check if it (or any of its subsets) also satisfies the other structures. If so, this solution is excluded and a new one is generated until all solutions are exhausted. Therefore, it is possible that SAT designs with 3 species satisfy all constraints but require significant computational resources to find them using this method.

We note that the range of parameters where the snub dodecahedron is formed enlarges, but not as much as in the case of the icosahedron or of the snub cube. In fact, the snub dodecahedron is not as robust to geometrical frustrations as the other structures. As γ approaches 90°, snub cubes start forming due to geometrical incompatibilities, but given the coloring, they never fully close. These almost complete structures require a large amount of time to break.

D. Short-Time Kinetics.

Here, we explore the effect of coloring on the short-time kinetics of the self-assembly process using Molecular Dynamics. We use a continuum version of the Kern–Frenkel potential and focus on the assembly process of the icosahedron. We restrict all results below to $\rho = 0.1$ and $T = 0.097$, as used in the previous sections. We also fix $\cos\theta_{max} = 0.97$ and $\gamma = 60°$ to more easily target the icosahedral shell. More detailed information regarding the
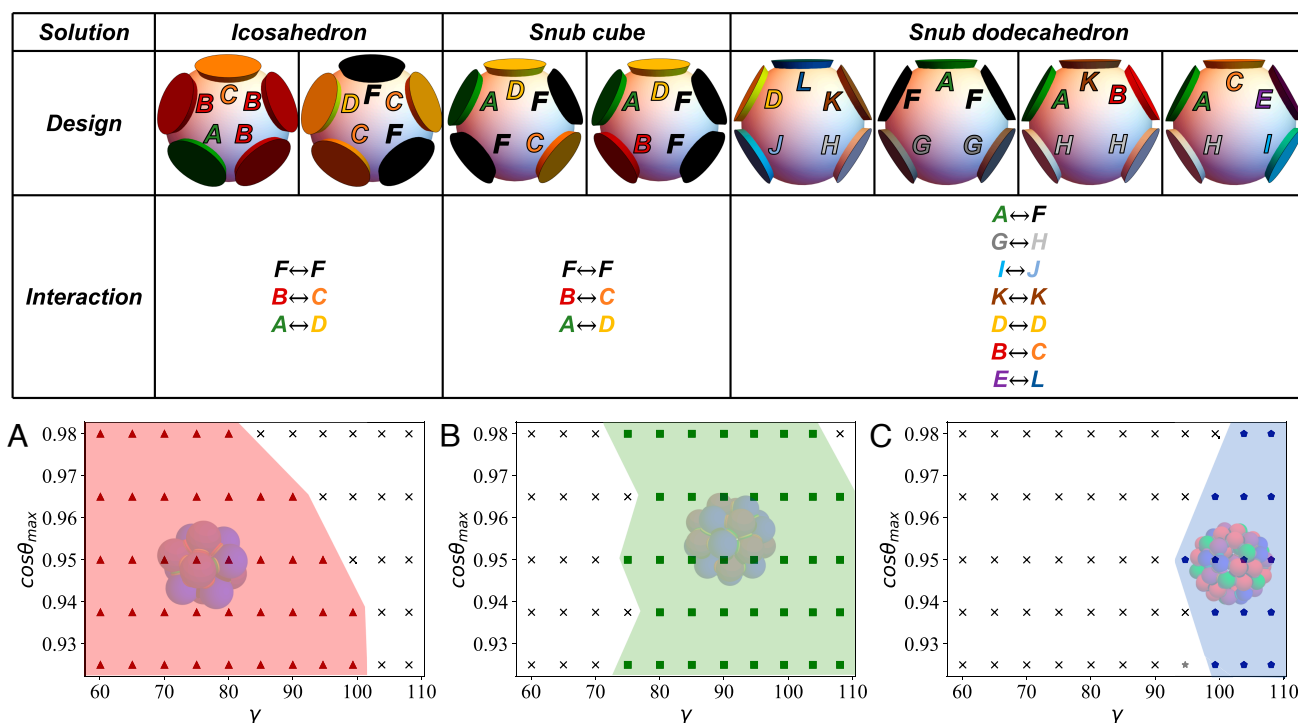

Fig. 5. *Top* Table: Graphic representation of the different multiparticle SAT solutions explored in this study, clarifying the respective patch coloring and interactions rules. Additional information regarding the designs is reported in *SI Appendix*. Panels (*A*), (*B*), and (*C*) show the most probable structure formed for different in-plane angles, γ, and for different patch width, $\cos\theta_{max}$, each for one specific SAT design. Panel (*A*) is based on a two-species and five-colors design, which allows the formation only of the icosahedron. Panel (*B*) is also based on a two-species and five-colors design, but which allows only the formation of the snub cube. Finally, (*C*) describes a four-species and twelve-colors SAT solution for which fully bonded configurations can be achieved only in the snub dodecahedron geometry. As for the previous figures, the colored areas indicate regions of the parameter space where self-assembly of the desired structure is successful. Results were calculated with $T = 0.097$ and $\rho = 0.01$. Temperature (*T*) is expressed in units of ϵ and $k_B = 1$, while all lengths are in units of σ.

https://doi.org/10.1073/pnas.2219458120

Molecular Dynamics simulations is presented in *Material and Methods*.

We focus on 10 different SAT solutions for the icosahedral shell and test for each of them the associated short-time kinetics. The first five correspond to solutions that have one species and an increasing number of colors: according to the nomenclature of Fig. 4, they are C1, C2(2), C3(2), C4(2), and C5. The remaining 5 solutions increase the number of species and use the corresponding maximum number of colors, in order C10 (2 species), C15 (3 species), C20 (4 species), C30 (6 species), and C60 (12 species).

Fig. 6 plots the fraction of monomers (nonbonded particles), P_1, as a function of time for the 10 different explored SAT solutions. We observe that adding more colors and species slows down the short-time kinetics of the system. Thus, it will take longer to reach the equilibrium state. To quantify this slowdown, we use the Smoluchowski coagulation equation to calculate the short-time aggregation rates (51, 52) and extend it to take into account the effect of coloring. In particular, we write

$$\frac{dP_1}{dt} = -K\rho P_1(t)P_1(t). \qquad [1]$$

We compute the aggregation rate K from the short-term fits of the solution of Eq. **1**,

$$P_1(t) = \frac{1}{1+K\rho t}, \qquad [2]$$

shown as dashed curves in Fig. 6. The inset of Fig. 6 shows the aggregation rate K plotted as a function of the number of colors. For isotropic particles, the Smoluchowski coagulation theory predicts $K = 8\pi D\sigma$, where D is the diffusion coefficient and σ is the diameter of the particle. To extend this to colored patchy particles, we write

$$K = 8\pi D\sigma \chi^2 \mathcal{C}, \qquad [3]$$

where $\chi = (1-\cos\theta_{max})/2$ is the fraction of the particle surface covered by a single patch and $\mathcal{C}$ is the number of bond

combinations among two particles allowed by the interaction matrix. For the C1 design (all patches having the same color), there are $\mathcal{C}_{C1} = 25$ possible bond combinations between two particles (each patch in the first particle can interact with each patch on the second particle). For C2(2), as seen in Fig. 4, 3 green patches on the first particle can interact with 3 green patches on the second particle (for a total of 9 combinations), while the 2 red patches on the first particle interact only with 2 red patches on the second particle (for a total of 4 combinations), giving $\mathcal{C}_{C2(2)} = 13$. With similar considerations, one finds that $\mathcal{C}_{C3(2)} = 9$, $\mathcal{C}_{C4(2)} = 7$, and $\mathcal{C}_{C5} = 5$. Full colored solutions ($N_c = 5N_p$) follow the simple rule $\mathcal{C}_{N_p} = 5/N_p = 25/N_c$, i.e., the aggregation rate scales as the inverse number of colors used.

In the *Inset* of Fig. 6, we plot the aggregation rate K measured for two different densities ($\rho = 0.1$ and $\rho = 0.001$) and the theoretical line $K = 8\pi D(\sigma + \delta)\chi^2 \mathcal{C}$. We observe that the simulations approach the theoretical prediction as the system becomes more diluted. We also see that even at high densities, the aggregation rate obeys the scaling law $K \approx N_c^{-1}$.

4. Conclusions

In this work, we have explored design principles that can guide the formation of complex target structures and applied them to regular polyhedral shells of valence five, i.e., the icosahedron, the snub cube, and the snub dodecahedron. In particular, we have explored how the interparticle interactions can encode a predetermined target structure, a strategy that has many counterparts in the biological world, as for example in the self-assembly of virus capsids.

Choosing the correct interparticle designs (i.e., patch coloring) is a complex optimization problem that we solve by encoding the bond topology in a set of satisfiability equations. This approach, named SAT-assembly, not only efficiently searches the space of possible designs for solutions which have the target structure as an energy minima, but also allows to explicitly enforce the nonsatisfiability of competing structures as a way of avoiding the formation of kinetic aggregates.

Starting from solutions which target at the same time all the structure of interest, we have explored the effects of patch geometry, patch coloring, and patch patterning on the aggregate's yield. We find that the symmetry of the building blocks plays a key role in determining the yield of the final structure, with chiral designs consistently producing high yields for all structures considered. Introducing frustration by altering the patch geometry from the ideal one is a promising strategy to produce designs with target structures that depend on external conditions.

We used SAT to selectively target one structure while excluding competing ones. For this, we increased the complexity of the design to two particle species and five patch colors for the icosahedron and snub cube, and four species and twelve colors for the snub dodecahedron. For these designs, we observe that the yield significantly increases (to almost 100% in multiple regions of the parameter space) and we also find a wider parameter range where it is possible to successfully assemble these structures. Thus, using SAT to suppress competing structures is a quite promising strategy for high-yield assemblies.

We have also explored the short-time kinetics of the icosahedral shell for different designs that vary in number of colors and species. Using the Smoluchowski coagulation equation, we show that the short-time kinetics slows down with increasing number of colors, with an inverse proportionality law. Since the static yield
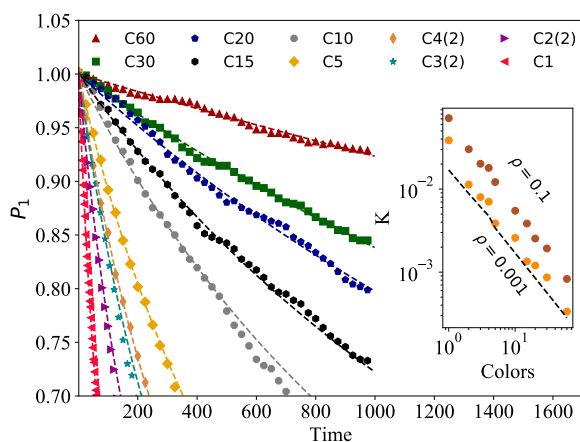

Fig. 6. Short-time kinetics of the icosahedron assembly for different numbers of species and colors. The main plot shows the time evolution of the fraction of monomers, $P_1(t)$, for short times using different designs with multiple species and colors. The lines are fits using $P_1(t) = 1/(1+K\rho t)$, with K as a fitting parameter and $\rho = 0.1$, for the short time scale of the kinetics (the fit is constrained to the range where P_1 is higher than 80%). The inset shows the aggregation rate as a function of the number of colors for two different densities, $\rho = 0.1$ and $\rho = 0.001$. We also show a theoretical line given by $K = 8\pi D(\sigma + \delta)\chi^2 \mathcal{C}$, with $D = 0.1$. All results were calculated using $T = 0.097$ and averaged over five independent samples.

saturates quickly with the number of colors, an optimal number of colors can be found that guarantees high yields in accessible experimental times. In this context, our assembly rules acquire even more significance because they show how to optimize the yield with changing color arrangement but without changing the overall number of colors (e.g., preferring chiral arrangements over nonchiral ones). For the respective capsid designs considered here, we observed nearly perfect yield with already just one species, making the use of more of them redundant. We notice also that increasing the number of different colors lowers the assembly temperature, potentially favoring—due to irreversible bonding—the formation of misfolded clusters. Hence, it is quite important to select in experiments the model that gives the required yield with the lowest number of colors. However, for other systems with fewer symmetries than the capsids considered here, the trade-off between number of species, desired yield, and assembly kinetics might result in a larger number of species and/or colors to be preferred (53).

Lastly, we also explored the phase diagram of these patchy particles designed with SAT (*SI Appendix*). We find a non-monotonous behavior of the average potential energy as a function of density, as is typical of self-assembly systems (42), where an ideal gas phase is found at very low densities, followed by a gas phase of clusters near the energy minima, ending at the liquid phase at high densities.

All the state diagrams shown in the main text were calculated using the same density and temperature. We expect that as long as the system remains in the same thermodynamic phase, the yield will remain almost constant. The results shown in Fig. 3 support this expectation since there the density was the control parameter. Of course, repeating the calculation with significantly higher temperatures will prevent the observation of clusters, since the system will be well below the critical miscelle concentration. Similarly, significantly lower temperatures can lead to large metastable clusters or even percolating ones that reduce the yield of the small shells. Thus, for the finite-size shells, the optimal yield should lie within an intermediate temperature range corresponding to the ideal gas phase of fully formed aggregates.

One of the possible pathways of realizing these designs experimentally is through 3D DNA nanomaterials, in particular wireframe DNA origami. Previous studies have successfully shown the versatility of these building blocks in assembling a wide array of structures (31–34). Recent work has achieved capsid assembly from 3D DNA origamis using shape complementary building blocks, akin to fitting puzzle pieces which bind at fixed prescribed angle (35). We note that our designs of colored patches can also be realized through the use of complementary strands, where compatible patch colors correspond to complementary DNA strands that functionalize the wireframe nanostructure to act as a patchy particle with selective spatial bonding and tune the interactions accordingly (16, 54). Such wireframe designs are expected to be easier to design than shape complementary origami and furthermore can be used as a reconfigurable system, which can form different target shapes based on which patch colors (DNA strands) are available. We also argue that our results support such approach not only due to the high yields observed in simulations but also due to the robustness of the structures formed to bonds with a high degree of angular flexibility, which is characteristic of DNA bonds (28, 55). Although we used an idealized patchy particle model, ongoing experimental DNA-origami results indicate that interaction designs based on simulations with this model can predict the structures obtained from the assembly of polyhedral DNA wireframes in experiments. Aside from flexible DNA wireframe origami, this type of design can be easily extended to proteins (56) or colloidal particles with brushes (20).

For simplicity, we allowed for self-complementary binding between patches. If such is not possible, adding more particle species is a simple way to introduce the noncomplementary bonding constraint. From what was shown here, we do not expect that such change should impact significantly the results, especially since it usually reduces the symmetry of the building blocks which promotes higher yields.

While we focused here in particular on three different shell designs, our design method could be straightforwardly applied to other capsid geometries, thus providing a computational pipeline of self-assembled shell designs for their possible nanotechnology applications.

Materials and Methods

We consider a system composed of N patchy particles in a cubic box of length L. Particles are characterized by a hard core of diameter σ with five patches on its surface. The patches interact through the Kern–Frenkel potential (49, 50):

$$V_{pp}(r_{ij}, \hat{r}_{\alpha,i}, \hat{r}_{\beta,j}) = V_{SW}(r_{ij})f(r_{ij}, \hat{r}_{\alpha,i}, \hat{r}_{\beta,j}), \quad [4]$$

where i corresponds to a given particle and r_i its center of mass. Thus, r_{ij} is the distance between particles i and j. $r_{\alpha,i}$ denotes the position of patch α of particle i. V_{SW} is an isotropic square-well of range $\sigma + \delta_{\alpha,\beta}$ and depth $\varepsilon_{\alpha,\beta}$, the hat symbol indicate unit vectors and f is the orientation-dependent modulation term that takes the form:

$$f(r_{ij}, \hat{r}_{\alpha,i}, \hat{r}_{\beta,j}) = \begin{cases} 1 & \text{if } \begin{array}{l} \hat{r}_{ij} \cdot \hat{r}_{\alpha,i} > \cos\theta_{\alpha\beta}^{\max} \\ \hat{r}_{ji} \cdot \hat{r}_{\beta,j} > \cos\theta_{\alpha\beta}^{\max} \end{array} \\ 0 & \text{otherwise.} \end{cases} \quad [5]$$

With this formulation, patches are represented by a cone starting from the center of mass of the particle and reaching $\sigma + \delta_{\alpha,\beta}$, while the width is controlled by $\theta_{\alpha\beta}^{\max}$ (as shown in Fig. 7). This potential has been extensively used to study systems of patchy particles (44). For simplicity, we consider the parameter range where it is only possible to form one bond per patch. In the following, σ provides the unit of length and $\varepsilon_{\alpha,\beta}$ the unit of energy. Temperature (T) is also expressed in units of $\varepsilon_{\alpha,\beta}$ and $k_B = 1$.

For the following results, we considered Monte Carlo (MC) simulations with two possible moves, roto-translations and aggregation-volume-bias (44). The first attempts a simple rotation and translation of a random particle along a random (radial or angular) direction. The second attempts to move a random particle into the vicinity of another such that a bond is formed between the two. To not break ergodicity, the inverse move can also be performed where a random bond between two particles is broken. We performed simulations
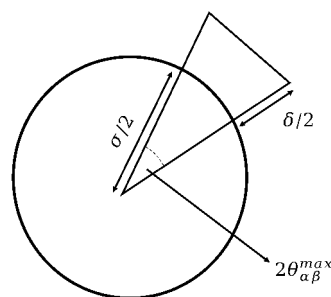

Fig. 7. Schematic representation of the Kern–Frenkel potential using the cross-section of a particle.

in the *NVT* assemble to explore the assembly of our desired shells. All results shown below were averages over simulations with or more than 10^8 MC time steps. For all, we considered $N = 480$ and $\delta_{\alpha,\beta} = 0.2$. The simulations start with particles randomly generated in the box with random orientations. Unless stated otherwise, all results are averages over 10 independent samples.

We follow the same SAT formulation as the one in ref. 38. We consider that each patch can have a given color, x_c, between $1 \leq x_c \leq N_c$, where N_c is the total number of colors. These colors can be distributed onto the patches in specific arrangements, each unique sequence can be considered a particle species, x_p, thus $1 \leq x_p \leq N_p$, where N_p is the total number of species. SAT is then used to find if a given combination of N_p and N_c can satisfy a given polyhedral shell, e.g., if it satisfies all the topological constraints, and a solution/design is calculated, which can be used to prepare the composition of the system. In *SI Appendix*, we go into more detail on the different constraints (clauses) used in SAT.

In Fig. 1, we show schematically one of the patchy particles of valence five used and the different shells assembled. There are three possible polyhedron shells that can form and fully close, depending on the parameters and SAT solution used: the regular icosahedron, the snub cube, and the snub dodecahedron. The positions of the five patches, for the case of the icosahedron, in the orthonormal base associated with the patchy particle, are given as:

$$\mathbf{p}_1 = \left(-\sqrt{\frac{\varphi + 2}{5}}, 0, \frac{\varphi - 1}{\sqrt{3 - \varphi}} \right)$$

$$\mathbf{p}_2 = \left(\frac{1 - \varphi}{2} \sqrt{\frac{\varphi + 2}{5}}, -\frac{\varphi}{2}, \frac{\varphi - 1}{\sqrt{3 - \varphi}} \right)$$

$$\mathbf{p}_3 = \left(\frac{\varphi}{2} \sqrt{\frac{\varphi + 2}{5}}, -\frac{1}{2}, \frac{\varphi - 1}{\sqrt{3 - \varphi}} \right) \quad [6]$$

$$\mathbf{p}_4 = \left(\frac{\varphi}{2} \sqrt{\frac{\varphi + 2}{5}}, \frac{1}{2}, \frac{\varphi - 1}{\sqrt{3 - \varphi}} \right)$$

$$\mathbf{p}_5 = \left(\frac{1 - \varphi}{2} \sqrt{\frac{\varphi + 2}{5}}, \frac{\varphi}{2}, \frac{\varphi - 1}{\sqrt{3 - \varphi}} \right),$$

where φ is the golden ratio. To form the other structures, one can increase the in-plane angle, γ, between $\mathbf{p}_4$ and $\mathbf{p}_5$. We do that by using $\mathbf{p}_3$ as an axis of rotation for $\mathbf{p}_4$ and $\mathbf{p}_1$ as an axis of rotation for $\mathbf{p}_5$. We multiply $\mathbf{p}_4$ and $\mathbf{p}_5$ by the respective rotation matrix, Eq. **7**, where $\mathbf{p}_{x,\alpha}$ refers to the rotation axis vector and α the vector index. The angle of rotation θ is used to increase the in-plane

angle γ. At $\theta = 0$, the in-plane angle is $\gamma = 60°$, while at $\theta \approx -46.5$ (and $\theta \approx 46.5$ for $\mathbf{p}_5$) the in-plane angle reaches the maximum value used of $\gamma \approx 108°$.

$$\begin{bmatrix} \sqrt{\mathbf{p}_{x,1}} + (1 - \sqrt{\mathbf{p}_{x,1}})\cos\theta & \mathbf{p}_{x,1}\mathbf{p}_{x,2}(1 - \cos\theta) - \mathbf{p}_{x,3}\sin\theta & \mathbf{p}_{x,1}\mathbf{p}_{x,3}(1 - \cos\theta) + \mathbf{p}_{x,2}\sin\theta \\ \mathbf{p}_{x,1}\mathbf{p}_{x,2}(1 - \cos\theta) + \mathbf{p}_{x,3}\sin\theta & \sqrt{\mathbf{p}_{x,2}} + (1 - \sqrt{\mathbf{p}_{x,2}})\cos\theta & \mathbf{p}_{x,2}\mathbf{p}_{x,3}(1 - \cos\theta) - \mathbf{p}_{x,1}\sin\theta \\ \mathbf{p}_{x,1}\mathbf{p}_{x,3}(1 - \cos\theta) - \mathbf{p}_{x,2}\sin\theta & \mathbf{p}_{x,2}\mathbf{p}_{x,3}(1 - \cos\theta) + \mathbf{p}_{x,1}\sin\theta & \sqrt{\mathbf{p}_{x,3}} + (1 - \sqrt{\mathbf{p}_{x,3}})\cos\theta \end{bmatrix} \quad [7]$$

Using SAT, we can find a minimal design that satisfies all three structures. For example, it is possible to consider the case that is shown in Fig. 1, where we only use one species (blue) of particles and two colors (green and red) for patches. In this design, green patches only interact with green and red with red. If the particles follow this coloring and interactions, then all three structures can in principle form. The SAT solution that leads to this design is not necessarily the only one that satisfies all structures but SAT only provides one solution at a time for the constraints provided. Nonetheless, SAT is flexible enough, such that, we can provide this solution found as another constraint and thus avoid a previous solution altogether. This leads to different solutions (translating into different particle designs). This process can be iterated until all solutions are exhausted.

One of the advantages of the SAT algorithm is that due to its high efficiency, it can be easily integrated into a simulation pipeline to quickly develop a design that excludes the maximum number of shells. Fig. 8 shows the relevant steps of this pipeline. One starts by using SAT to calculate a solution that satisfies the targeted shell. Then, the system is simulated using this design to find new misfolded shells different from the target one. These misfolded shells are then added to SAT and excluded from the new solution. Thus, those misfolded shells will no longer form. This process can be iterated until the yield of misfolded shells is negligible. For the geometry of patchy particles presented in this article, the three main closed shells are the ones in Fig. 1. For the range of parameters explored, the misfolded shells have very low yields or are constrained to limits of the parameter space (wide patch widths). Thus, in the present case, the path in Fig. 8 coincides with the straight line connecting the blue to the green box.

The short-time assembly simulations were performed using a Molecular Dynamics method with a generalization of the Kern–Frenkel potential between patches (39). Patchy particles feel a mutual repulsion modeled through a WCA interaction:

$$U_{ij}(r) = \begin{cases} 4\varepsilon \left[\left(\frac{\sigma}{r}\right)^{12} - \left(\frac{\sigma}{r}\right)^{6} + \frac{1}{4} \right] & r \leq 2^{\frac{1}{6}}\sigma \\ 0 & r > 2^{\frac{1}{6}}\sigma \end{cases}, \quad [8]$$
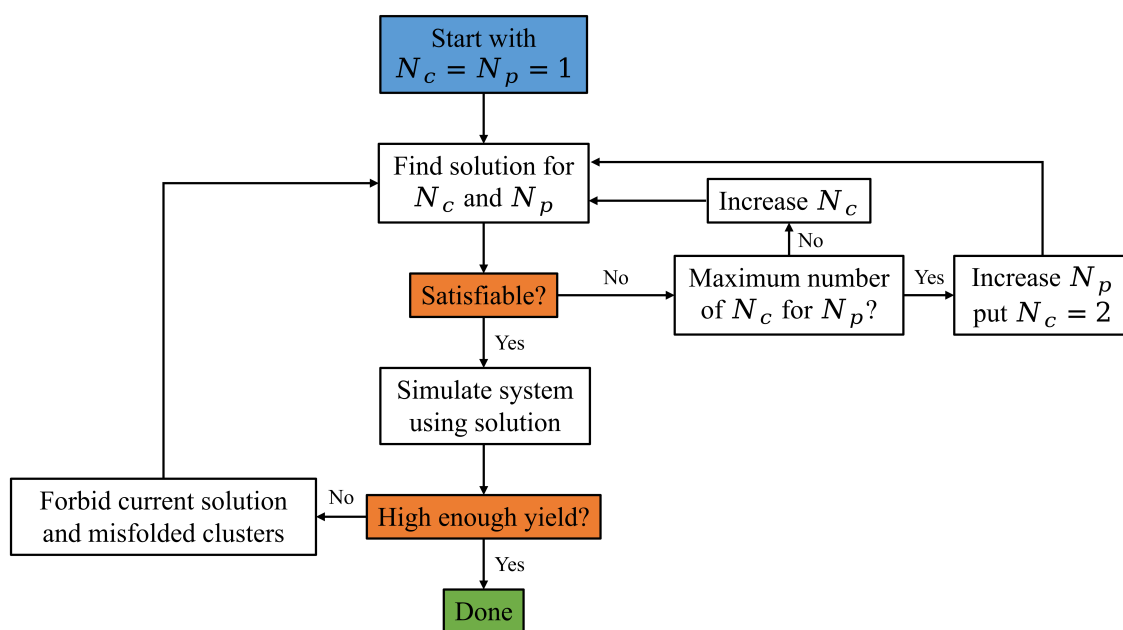

Fig. 8. Diagram of the SAT pipeline.

where r is the distance between particle centers, ε is the energy scale, and σ is the particle diameter. Thus, energy is in units of ε while lengths are in units of σ.

The patch–patch interaction is a square-well-like attractive potential modulated by an orientation-dependent function. The range of the interaction is given by δ, while its angular width is given by $\cos\theta_{max}$. The interaction between patch i on particle α, identified by the unit vector $\hat{\alpha}_i$, and patch j on particle β, identified by $\hat{\beta}_j$, is given by

$$V_{pp}(\vec{r}_{pp}, \hat{\alpha}_i, \hat{\beta}_j) = -\varepsilon \exp\left(-\frac{1}{2}\left(\frac{r_{pp} - \sigma_c}{\delta}\right)^{10}\right) \Omega(-\hat{r}, \hat{\alpha}_i)\Omega(\hat{r}_{pp}, \hat{\beta}_j),$$

[9]

where $\vec{r}_{pp} = \vec{r}_\alpha - \vec{r}_\beta$, $r_{pp} = |\vec{r}_{pp}|$, $\hat{r}_{pp} = \vec{r}_{pp}/r_{pp}$ and Ω is a steep modulating function that takes into account the orientation of a patch with respect to the unit vector connecting the center of the particles and takes the following form:

$$\Omega(\hat{r}, \hat{\gamma}_k) = \exp\left(-\frac{1}{2}\left(\frac{1 - \hat{r} \cdot \hat{\gamma}_k}{1 - \cos\theta_{max}}\right)^{20}\right).$$

[10]

We set $\delta = 0.2$ and $\cos\theta_{max} = 0.97$ so that only one bond can form per patch. We used the oxDNA package (57, 58) to simulate the patchy particle system described above. We only focused on the icosahedral shell, so the patches were located at the positions given by Eq. 6.

Data, Materials, and Software Availability. The code implementing the SAT-assembly pipeline for polyhedral shells is available at https://github.com/deppinto/PatchyParticles. The data used in the results shown can be found in https://doi.org/10.5281/zenodo.7787992 (59).

Author affiliations: [a]Dipartimento di Fisica, Sapienza Università di Roma, Rome 00185, Italy; [b]Life and Medical Sciences (LIMES), University of Bonn, Bonn 53121, Germany; and [c]School of Molecular Sciences and Center for Molecular Design and Biomimetics, The Biodesign Institute, Arizona State University, Tempe, AZ 85281

1. S. Whitelam, R. L. Jack, The statistical mechanics of dynamic pathways to self-assembly. *Ann. Rev. Phys. Chem.* **66**, 143–163 (2015).
2. G. M. Whitesides, B. Grzybowski, Self-assembly at all scales. *Science* **295**, 2418–2421 (2002).
3. A. J. Parnell *et al.*, Spatially modulated structural colour in bird feathers. *Sci. Rep.* **5**, 18317 (2015).
4. J. Teyssier, S. V. Saenko, D. van der Marel, M. C. Milinkovitch, Photonic crystals cause active colour change in chameleons. *Nat. Commun.* **6**, 6368 (2015).
5. M. Martín-Bravo, J. M. G. Llorente, J. Hernández-Rojas, D. J. Wales, Minimal design principles for icosahedral virus capsids. *ACS Nano* **15**, 14873–14884 (2021).
6. M. F. Hagan, D. Chandler, Dynamic pathways for viral capsid assembly. *Biophys. J.* **91**, 42–54 (2006).
7. N. V. Dziomkina, G. J. Vancso, Colloidal crystal assembly on topologically patterned templates. *Soft. Matter.* **1**, 265–279 (2005).
8. S. C. Glotzer, M. J. Solomon, Anisotropy of building blocks and their assembly into complex structures. *Nat. Mater.* **6**, 557–562 (2007).
9. S. H. Kim, S. Y. Lee, S. M. Yang, G. R. Yi, Self-assembled colloidal structures for photonics. *NPG Asia Mater.* **3**, 25–33 (2011).
10. R. A. LaCour, T. C. Moore, S. C. Glotzer, Tuning stoichiometry to promote formation of binary colloidal superlattices. *Phys. Rev. Lett.* **128**, 188001 (2022).
11. R. McGorty, J. Fung, D. Kaz, V. N. Manoharan, Colloidal self-assembly at an interface. *Mater. Today* **13**, 34–42 (2010).
12. Y. Mu *et al.*, Binary phases and crystals assembled from active and passive colloids. *ACS Nano* **16**, 6801–6812 (2022).
13. D. Nykypanchuk, M. M. Maye, D. van der Lelie, O. Gang, DNA-guided crystallization of colloidal nanoparticles. *Nature* **451**, 549–552 (2008).
14. S. Sacanna, D. J. Pine, Shape-anisotropic colloids: Building blocks for complex assemblies. *Curr. Opin. Colloid Interface Sci.* **16**, 96–105 (2011).
15. Y. Wang *et al.*, Colloids with valence and specific directional bonding. *Nature* **491**, 51–55 (2012).
16. Y. Wang *et al.*, Crystallization of DNA-coated colloids. *Nat. Commun.* **6**, 7253 (2015).
17. D. Joshi *et al.*, Kinetic control of the coverage of oil droplets by DNA-functionalized colloids. *Sci. Adv.* **2**, e1600881 (2016).
18. K. J. M. Bishop, Self-assembly across scales. *Nat. Mater.* **21**, 501–502 (2022).
19. D. Reguera, J. Hernández-Rojas, J. M. Gomez Llorente, Kinetics of empty viral capsid assembly in a minimal model. *Soft. Matter.* **15**, 7166–7172 (2019).
20. A. McMullen, M. Muñoz Basagoiti, Z. Zeravcic, J. Brujic, Self-assembly of emulsion droplets through programmable folding. *Nature* **610**, 502–506 (2022).
21. A. W. Wilber *et al.*, Reversible self-assembly of patchy particles into monodisperse icosahedral clusters. *J. Chem. Phys.* **127**, 085104 (2007).
22. D. J. Kraft *et al.*, Surface roughness directed self-assembly of patchy particles into colloidal micelles. *Proc. Natl. Acad. Sci. U.S.A.* **109**, 10787–10792 (2012).
23. H. W. Hatch, S. Y. Yang, J. Mittal, V. K. Shen, Self-assembly of trimer colloids: Effect of shape and interaction range. *Soft. Matter.* **12**, 4170–4179 (2016).
24. J. D. Halverson, A. V. Tkachenko, DNA-programmed mesoscopic architecture. *Phys. Rev. E* **87**, 062310 (2013).
25. D. Frenkel, D. J. Wales, Designed to yield. *Nat. Mater.* **10**, 410–411 (2011).
26. M. H. Lash, M. V. Fedorchak, J. J. McCarthy, S. R. Little, Scaling up self-assembly: Bottom-up approaches to macroscopic particle organization. *Soft. Matter.* **11**, 5597–5609 (2015).
27. A. van Blaaderen, Colloids get complex. *Nature* **439**, 545–546 (2006).
28. S. A. J. van der Meulen, M. E. Leunissen, Solid colloids with surface-mobile DNA linkers. *J. Am. Chem. Soc.* **135**, 15129–15134 (2013).
29. X. Huang *et al.*, Self-assembled virus-like particles with magnetic cores. *Nano Lett.* **7**, 2407–2416 (2007).
30. M. Uchida *et al.*, Biological containers: Protein cages as multifunctional nanoplatforms. *Adv. Mater.* **19**, 1025–1042 (2007).
31. M. Mosayebi *et al.*, Beyond icosahedral symmetry in packings of proteins in spherical shells. *Proc. Natl. Acad. Sci. U.S.A.* **114**, 9014–9019 (2017).
32. J. G. Lee, K. S. Kim, J. Y. Lee, D. N. Kim, Predicting the free-form shape of structured DNA assemblies from their lattice-based design blueprint. *ACS Nano* **16**, 4289–4297 (2022).
33. H. Jun *et al.*, Rapid prototyping of arbitrary 2D and 3D wireframe DNA origami. *Nucleic Acids Res.* **49**, 10265–10274 (2021).
34. P. W. Rothemund, Folding DNA to create nanoscale shapes and patterns. *Nature* **440**, 297–302 (2006).
35. C. Sigl *et al.*, Programmable icosahedral shell system for virus trapping. *Nat. Mater.* **20**, 1281–1289 (2021).
36. P. R. ten Wolde, D. Frenkel, Enhancement of protein crystal nucleation by critical density fluctuations. *Science* **277**, 1975–1978 (1997).
37. F. Romano, J. Russo, L. Kroc, P. Šulc, Designing patchy interactions to self-assemble arbitrary structures. *Phys. Rev. Lett.* **125**, 1–6 (2020).
38. J. Russo *et al.*, SAT-assembly: A new approach for designing self-assembling systems. *J. Phys.: Condens. Matter.* **34**, 354002 (2022).
39. L. Rovigatti *et al.*, A simple solution to the problem of self-assembling cubic diamond crystals. *Nanoscale* **14**, 14268–14275 (2022).
40. Z. Zhang, S. C. Glotzer, Self-assembly of patchy particles. *Nano Lett.* **4**, 1407–1413 (2004).
41. E. Bianchi, J. Largo, P. Tartaglia, E. Zaccarelli, F. Sciortino, Phase diagram of patchy colloids: Towards empty liquids. *Phy. Rev. Lett.* **97**, 168301 (2006).
42. F. Sciortino, A. Giacometti, G. Pastore, Phase diagram of Janus particles. *Phys. Rev. Lett.* **103**, 237801 (2009).
43. F. Romano, E. Sanz, F. Sciortino, Phase diagram of a tetrahedral patchy particle model for different interaction ranges. *J. Chem. Phys.* **132**, 184501 (2010).
44. L. Rovigatti, J. Russo, F. Romano, How to simulate patchy particles. *Eur. Phys. J. E* **41**, 59 (2018).
45. J. Russo, F. Leoni, F. Martelli, F. Sciortino, The physics of empty liquids: From patchy particles to water. *Rep. Prog. Phys.* **85**, 016601 (2022).
46. A. B. Pawar, I. Kretzschmar, Fabrication, assembly, and application of patchy particles. *Macromol. Rapid Commun.* **31**, 150–168 (2010).
47. S. Ravaine, E. Duguet, Synthesis and assembly of patchy particles: Recent progress and future prospects. *Curr. Opin. Colloid Interface Sci.* **30**, 45–53 (2017).
48. S. C. Harrison, Looking inside adenovirus. *Science* **329**, 1026–1027 (2010).
49. N. Kern, D. Frenkel, Fluid-fluid coexistence in colloidal systems with short-ranged strongly directional attraction. *J. Chem. Phys.* **118**, 9882 (2003).
50. W. Bol, Monte Carlo simulations of fluid systems of waterlike molecules. *Mol. Phys.* **45**, 605–616 (1982).
51. F. Sciortino *et al.*, A parameter-free description of the kinetics of formation of loop-less branched structures and gels. *Soft Matter* **5**, 2571–2575 (2009).
52. N. Ghofraniha, P. Andreozzi, J. Russo, C. La Mesa, F. Sciortino, Assembly kinetics in binary mixtures of strongly attractive colloids. *J. Phys. Chem. B* **113**, 6775–6781 (2009).
53. J. Bohlin, A. J. Turberfield, A. A. Louis, P. Šulc, Designing the self-assembly of arbitrary shapes using minimal complexity building blocks. *ACS Nano* **17**, 5387–5398 (2023).
54. P. L. Biancaniello, A. J. Kim, J. C. Crocker, Colloidal interactions and self-assembly using DNA hybridization. *Phys. Rev. Lett.* **94**, 058302 (2005).
55. N. Geerts, E. Eiser, DNA-functionalized colloids: Physical properties and applications. *Soft. Matter* **6**, 4647 (2010).
56. J. Zhu *et al.*, Protein assembly by design. *Chem. Rev.* **121**, 13701–13796, PMID: 34405992 (2021).
57. L. Rovigatti, P. Šulc, I. Reguly, F. Romano, A comparison between parallelization approaches in molecular dynamics simulations on GPUs. *J. Comput. Chem.* **36**, 1–8 (2015).
58. E. Poppleton *et al.*, OxDNA: Coarse-grained simulations of nucleic acids made simple. *J. Open Source Softw.* **8**, 4693 (2023).
59. D. E. P. Pinto, Design strategies for the self-assembly of polyhedral shells. Zenodo. https://zenodo.org/record/7787992#.ZClG93axWUl. Deposited 31 March 2023.